

Magnetization study of the ultra-hard material MgAlB_{14}

J.M. Hill^{a,*}, D.C. Johnston^a, B.A. Cook^b, J.L. Harringa^b, A.M. Russell^b

^aAmes Laboratory and Department of Physics and Astronomy, Iowa State University, Ames, IA 50011, USA

^bAmes Laboratory, Iowa State University, Ames, IA 50011, USA

Received 5 December 2002

Abstract

Magnetic susceptibility χ versus temperature T , magnetization M versus T , and isothermal M versus magnetic field H studies of the ultra-hard material MgAlB_{14} were carried out in search of superconductivity or ferromagnetism in this compound. Two types of samples were synthesized: (1) powder and (2) chemically substituted and unsubstituted hot pressed pellets prepared from mechanically alloyed powders. $\chi(T)$ measurements on a powder sample revealed temperature-independent diamagnetism with a Curie–Weiss impurity concentration equivalent to ~ 1 mol% of spin- $\frac{1}{2}$ ions. In contrast, $M(T)$ and $M(H)$ data on the hot pressed samples, both substituted and unsubstituted, showed evidence of ferromagnetic transitions above ~ 330 K. Scanning electron microscopy and Auger microprobe analysis of the hot pressed samples indicated that both substituted and unsubstituted samples contained significant concentrations of Fe impurities. We conclude that pure MgAlB_{14} is neither a superconductor nor a ferromagnet above 1.8 K and exhibits temperature-independent diamagnetism from 1.8 K up to room temperature. The ferromagnetism observed in the hot pressed samples is likely due to Fe impurities abraded from the stainless steel mills used to mix the starting materials prior to hot pressing the samples.

© 2003 Elsevier Science B.V. All rights reserved.

PACS: 75.20.-g; 75.30.Cr; 81.05.Je; 81.40.Rs

Keywords: Ultra-hard boride MgAlB_{14} ; Magnetization measurements; Ferromagnetic impurities

1. Introduction

The recent discovery by Akimitsu and co-workers of superconductivity at 39 K in MgB_2 [1] indicated that the condensed matter physics community may have overlooked interesting physical properties in other known non-transition metal compounds. Initial studies of MgB_2 [2] provided strong evidence that it was a BCS [3]

superconductor. More recently, experiments have shown that high frequency phonons are likely involved in the electron–phonon pairing interaction [4,5]. Materials with high phonon frequencies tend to have high Debye temperatures θ_D and more rigid elastic constants [6]. Masui et al. (Ref. [4]) have recently estimated θ_D to be ~ 400 K in MgB_2 . High rigidity is linked to the hardness of a material [7]. This suggests that other hard, non-transition metal compounds may also exhibit superconductivity.

Young et al. (Ref. [8]) discovered recently that single crystals of $\text{Ca}_{1-x}\text{La}_x\text{B}_6$ exhibited

*Corresponding author. Tel.: +515-294-1364; fax: +515-294-0689.

E-mail address: jmhill@ameslab.gov (J.M. Hill).

ferromagnetism with Curie temperatures up to ~ 600 K and very small saturation moments. This discovery generated much theoretical and experimental work on doped and undoped CaB_6 and SrB_6 . There are no transition metal atoms in either of these compounds, suggesting that the observed ferromagnetism arises from an as yet unknown mechanism. This discovery suggests that other boride compounds which do not contain transition metal atoms may also exhibit this new “exotic” ferromagnetism. However, recent results [9,10] provide strong evidence that the ferromagnetism observed in $\text{Ca}_{1-x}\text{La}_x\text{B}_6$ is due to ferromagnetic impurities present on the surface of the crystals.

Chemically modified MgAlB_{14} was discovered by Ames Laboratory scientists a few years ago to have a hardness ranging from 32–46 GPa, making it one of the hardest materials known [11]. For comparison, diamond, with a hardness of 70–100 GPa (Vickers Hardness Number = $8400 \text{ kg/mm}^2 = 82 \text{ GPa}$ [12]) and a θ_D of 1860 K [13], is the hardest bulk material known. MgAlB_{14} has an orthorhombic crystal structure containing B_{12} icosahedra arranged in distorted, close-packed layers linked together by the metal atoms and by single B atoms [14–16]. The partially (~ 0.8) occupied Al (Mg) sites form linear (zig-zag) chains parallel to the a -axis. The interatomic distances within the chains and between Mg and Al chains are comparable to the interatomic distances in Mg and Al metal [15,17]. Single crystal refinements of MAlB_{14} ($M = \text{Tb, Dy, Ho, Er, Tm, Yb, Lu, Y, Li}$) yielded similar results [17–19,16]. The compound Mg_2B_{14} was found by Guette et al. (Ref. [20]) to have the same orthorhombic structure but with a B/Mg ratio much closer to 7.

A few physical property studies have been reported in the literature for this boride family. Three studies reported that the temperature dependence of the Seebeck coefficient and electrical conductivity of polycrystalline MgAlB_{14} showed a simultaneous increase with temperature above 300 K, indicative of hopping conduction in a non-metallic, disordered system [21–23]. A recent study on polycrystalline samples by Takeda et al. (Ref. [24]) reported that the Seebeck coefficient decreased with increasing temperature and that the electrical conductivity increased with increasing

temperature. Mössbauer spectra for Fe-doped polycrystalline MgAlB_{14} , $\text{Fe}(\text{MgAlB}_{14})_{30}$, indicated that the Fe exists in two oxidation states, Fe^{+2} and Fe^{+3} , in this material [23]. The temperature dependencies of the Seebeck coefficient and electrical conductivity for $\text{Fe}(\text{MgAlB}_{14})_{30}$ were unchanged from those of the Fe-free materials [23]. Infrared spectroscopy measurements on a single crystal of MgAlB_{14} were also consistent with non-metallic behavior [25]. Measurements on less disordered MgAlB_{14} samples which contain no metal atom vacancies would help to clarify the conduction mechanism in this compound.

Magnetization measurements ranging from 5–280 K on polycrystalline $\text{M}_{1-x}\text{Al}_{1-y}\text{B}_{14}$ ($M = \text{Tb, Dy, Ho, Er}$) samples indicated local moment magnetism consistent with the magnetism of trivalent rare earth ions [17]. The magnetic susceptibility followed the Curie–Weiss law, $\chi = C/(T - \theta)$, where the Curie constant is $N\mu_{\text{eff}}^2/3k_B$; N is the number of magnetic atoms, μ_{eff} is the effective magnetic moment per rare earth atom, and k_B is Boltzmann’s constant. The effective moments μ_{eff} obtained ranged from 11 to $12 \mu_B$, slightly larger than calculated values, and the obtained Weiss temperatures were $\theta \approx -15$ K for $M = \text{Dy, Ho, and Er}$, and 10 K for $M = \text{Tb}$. Measurements of the temperature dependence of the electrical resistance of a single crystal of $\text{Er}_{1-x}\text{Al}_{1-y}\text{B}_{14}$ were consistent with variable-range hopping [17]. This is in agreement with results discussed above which indicate that the electrical properties of MAlB_{14} are indicative of a non-metallic, disordered system.

In a search for superconductivity and/or ferromagnetism in the ultra-hard material MgAlB_{14} , we have measured the magnetization of hot pressed materials as well as a polycrystalline sample prepared using conventional solid state synthesis. The data for the powder sample are presented directly following the Experimental Details section below, followed by the data on hot pressed samples.

2. Experimental details

Powder samples of MgAlB_{14} were synthesized by reacting 99.999% pure (metals basis) distilled

Mg metal (Ames Laboratory), 99.999% Al spheres, and 99.99% amorphous B powder (Alfa Aesar) in sealed Ta tubes at 1300°C for approximately three weeks. Fast neutron activation analysis (Elemental Analysis, Inc.) revealed that the B powder, which was dried under vacuum at 600°C and subsequently handled and stored in a high-purity He atmosphere, was contaminated with 6.0(3) wt% of oxygen. Powder X-ray diffraction (XRD) patterns were taken on a Rigaku X-ray diffractometer with CuK α radiation. Fig. 1 shows the XRD pattern of a sample for which the starting materials were briefly exposed to air before sealing in the Ta tube. Lattice parameters were obtained from a different XRD pattern using Si powder as an internal standard. The XRD pattern showed that the sample consists of MgAlB₁₄, together with a significant amount of spinel, MgAl₂O₄, as the major impurity phase arising from the O impurities in the B powder starting material and possibly from exposing the reactants to air. The MgAlB₁₄ diffraction peaks (●) were indexed in the orthorhombic space group *Imam* (No. 74) with lattice parameters $a = 5.866(2)$ Å, $b = 8.114(5)$ Å, and $c = 10.312(6)$ Å, similar to literature values [15]. The impurity MgAl₂O₄ (20 ± 5 wt%) reflections are also indicated in the figure (○). Altering the synthesis

technique such that the reactants were not exposed to air before they were sealed into the Ta tube resulted in samples which had larger amounts of AlB₁₂ impurities as shown in Fig. 2. We could not identify all of the impurity phases present in the samples. Changing the Mg:Al:B stoichiometry of the starting materials from 1:1:14 to 1:1:10 or 0.8:0.8:14 did not affect the results. No single-phase samples were obtained using the synthesis method employed here.

Vekshina et al. (Ref. [26]) successfully removed impurity phases from their samples of powder MgAlB₁₄ by dissolving their boron-poor impurity phases and/or unreacted metals with boiling aqueous HCl. Therefore, we treated some samples with boiling 4 M HCl. However, the weight loss due to the acid treatment was negligible. In addition, the XRD patterns of a sample taken before the acid treatment and after the acid treatment were essentially identical, as shown in Fig. 3, with only minor changes in the intensity of some peaks. Treating the samples with NH₄OH also did not affect the phase composition of the samples. We conclude that the above chemical treatments of our samples had no significant effect on their phase composition.

Hot pressed samples of MgAlB₁₄ and MgAlB₁₄:X (X=Si, TiB₂) were prepared by mechanical alloying with hardened chrome steel

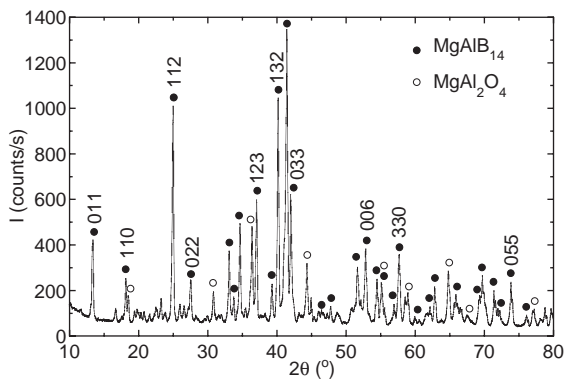


Fig. 1. X-ray powder diffraction pattern of MgAlB₁₄ (CuK α radiation). The solid curve is intensity I versus diffraction angle 2θ . The MgAlB₁₄ diffraction lines are indicated by ● and are indexed in the orthorhombic space group *Imam* (No. 74) with $a = 5.866(2)$ Å, $b = 8.114(5)$ Å, and $c = 10.312(6)$ Å. The Miller indices of the strongest reflections are shown. Impurity MgAl₂O₄ reflections are indicated by ○.

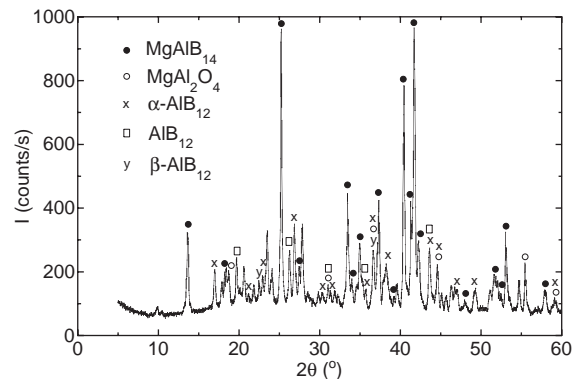


Fig. 2. X-ray powder diffraction pattern of MgAlB₁₄ (CuK α radiation). The solid curve is intensity I versus diffraction angle 2θ . The line positions for MgAlB₁₄ (●) and MgAl₂O₄ (○) are indicated. Reflections for α -AlB₁₂ (x), AlB₁₂ (□), and β -AlB₁₂ (y) are also marked.

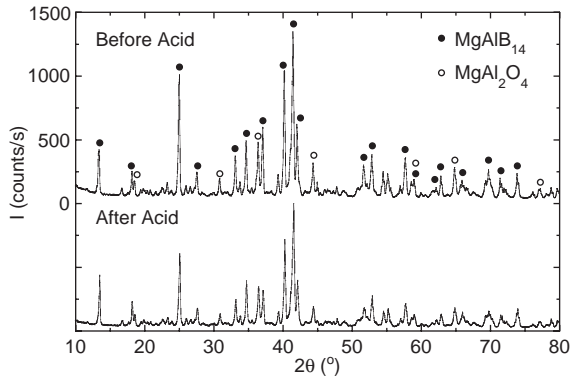


Fig. 3. X-ray powder diffraction pattern of MgAlB_{14} showing intensity I versus diffraction angle 2θ ($\text{CuK}\alpha$ radiation). The top curve was taken before treatment of the sample with boiling 4M HCl and the bottom curve was taken after the HCl treatment. MgAlB_{14} (MgAl_2O_4) line positions are indicated by \bullet (\circ). For clarity, the intensity of the bottom curve was shifted downwards by 1000 counts/s.

ball mills (Spex Industries) and consolidated by vacuum hot pressing at 1300–1500°C in BN-lined graphite dies as described in Ref. [27]. Some samples were examined for elemental content by two field emission electron microprobe instruments: a scanning electron microscope (SEM) (Amray) and a scanning Auger microprobe (Jeol JAMP-7830F). Fig. 4 shows a backscattered SEM picture of an unsubstituted hot pressed MgAlB_{14} sample, which is clearly inhomogeneous. Energy dispersive spectroscopy (EDS) analyses of spot “1” and spot “2” are shown in Fig. 5. For chemical analysis, the grain size of these materials is less than the minimum electron beam spot size ($\sim 1\mu\text{m}$). Therefore various multi-grain regions of overall homogeneous chemical composition over the $1\mu\text{m}$ spot area (as determined from z-contrast imaging) were analyzed. It is clear that the elemental content, particularly Fe, varies greatly with position in this material. The bright regions in Fig. 4 (spot 1) have a high Fe content, whereas the light gray areas (spot 2) have a much lower Fe content. EDS spectra from the dark gray areas gave identical results as from spot 2. Fe is evidently introduced into the material from milling wear debris. Light elements are not detected as efficiently by EDS as are the heavier elements.

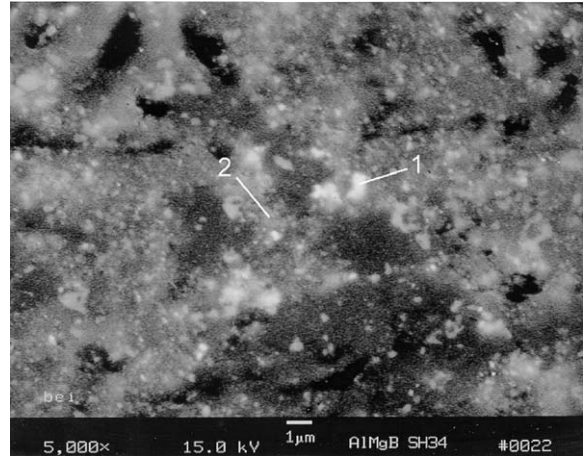


Fig. 4. Scanning electron microscope image of the microstructure of hot pressed MgAlB_{14} containing Fe, O, and C impurities (BSE mode). The brightest areas correspond to Fe enrichment. Energy dispersive spectroscopy spectra corresponding to two points (labeled “1” and “2”) on the micrograph are shown in Fig. 5.

Therefore, B, C, and O peak heights are not a reliable quantitative indication of their relative concentrations in this material.

In addition to the above analyses, a hot pressed sample prepared from powder precursor materials and nominally substituted with 0.63 at% Si for Al was etched with an Ar^+ ion beam before analysis in the Auger microprobe. Iron-rich precipitates are seen as bright phases against the dark matrix (MgAlB_{14} material) because of the high atomic number contrast, and were distributed across the surface of the specimen (not shown). Analysis of the Auger electron spectra obtained from several matrix regions gave an Al:Fe ratio of 46.7:9.54 at% (sensitivity to the B signal is poor and results are calculated with respect to all heavier elements). Since Al loss during the processing has been found to be negligible, this ratio can be directly scaled to the nominal Al concentration, with the result that the average Fe content within the matrix phase is 1.09 at%, corresponding to the approximate composition $(\text{MgAlB}_{14})\text{Fe}_{0.17}$.

Two additional samples were examined in the SEM. The first was another 0.63 at% Si-substituted composition, similar to the one

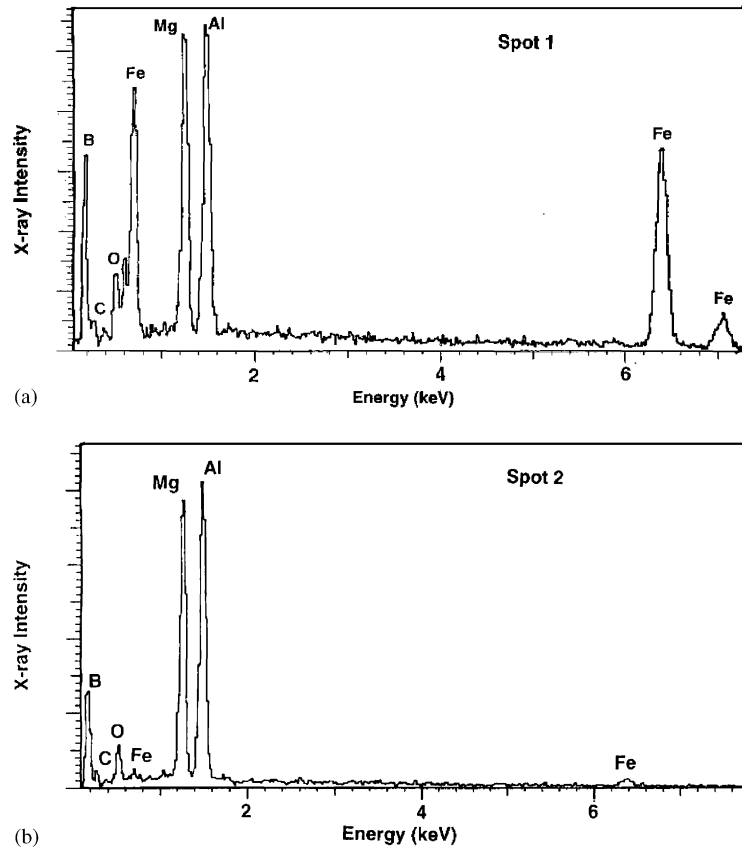


Fig. 5. Energy dispersive spectroscopy (EDS) spectra from the locations labeled 1 (a) and 2 (b) in Fig. 4. Fe and B contents vary with position in this material.

discussed above. Semi-quantitative EDS analysis of three matrix regions gave Fe concentrations of 0.88, 2.25, and 2.3 at%, for an average of 1.81 at%. Three regions within the second sample, an unsubstituted hot pressed MgAlB_{14} sample, gave results of 1.65, 1.62, and 1.91 at% Fe, for an average of 1.73 at%. It is expected that the majority of the Fe would be found as a second phase along MgAlB_{14} grain boundaries. Alternatively, these values place an upper limit on the amount of Fe substitutionally incorporated within the MgAlB_{14} phase to be about 1.8 at%.

Magnetic susceptibility χ versus temperature T and isothermal magnetization M versus magnetic field H measurements from 1.8 to 400 K were carried out using a Quantum Design MPMS

superconducting quantum interference device (SQUID) magnetometer.

3. Magnetization of polycrystalline powder MgAlB_{14}

The magnetization M versus magnetic field H isotherm at $T = 300$ K for our powder sample of MgAlB_{14} (see Fig. 1) is shown in Fig. 6. The saturation moment M_s was obtained by fitting the high field data with the fit function

$$M(H, T) = M_s(T) + \chi(T)H, \quad (1)$$

where $\chi(T)$ is the magnetic susceptibility, yielding $M_s = 4.05(5) \times 10^{-3} \text{ G cm}^3/\text{g}$, which is equivalent to the contribution of 18.2 wtppm of Fe metal

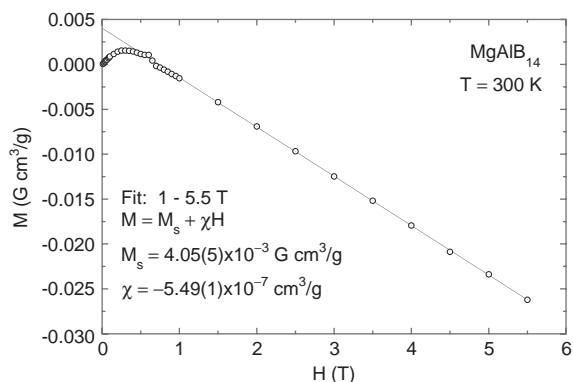


Fig. 6. Magnetization M versus magnetic field H of a MgAlB_{14} powder sample at 300 K (\odot). The solid curve is a fit to the high field data at $H \geq 1$ T by the function shown in the figure [Eq. (1)], with parameters also listed in the figure.

impurities, and $\chi = -5.49(1) \times 10^{-7} \text{ cm}^3/\text{g}$. Similar data taken at 50, 100, and 200 K showed that M_s increased only slightly to $M_s = 4.31(9) \times 10^{-3} \text{ G cm}^3/\text{g}$, allowing a fit to $M_s(T)$ to be made. Then we extracted the susceptibility $\chi(T)$,

$$\chi(T) = \frac{M(H, T) - M_s(T)}{H}, \quad (2)$$

from $M(T)$ at constant $H = 1$ T. $M(H, T)$ at $H = 1$ T is in the linear regime of the $M(H)$ plots, as shown in Fig. 6, which is necessary for the derived $\chi(T)$ to be valid.

The magnetic susceptibility $\chi(T)$ in an applied magnetic field of $H = 10$ kOe for a powder MgAlB_{14} sample which contained 20 ± 5 wt% MgAl_2O_4 , described above, is shown in Fig. 7. The ferromagnetic impurity contribution $M_s(T)$ to $M(H, T)$, from $M(H)$ isotherms taken from 50 to 300 K as described above, is corrected for in Fig. 7. The compound exhibits temperature-independent diamagnetism at high temperature with a small Curie–Weiss paramagnetic impurity contribution. We fitted the data by

$$\chi = \chi_0 + \frac{C_{\text{imp}}}{T - \theta}, \quad (3)$$

where θ is the Weiss temperature and C_{imp} is the impurity Curie constant. The T -independent χ_0 term,

$$\chi_0 = \chi^{\text{core}} + \chi^{\text{VV}} \quad (4)$$

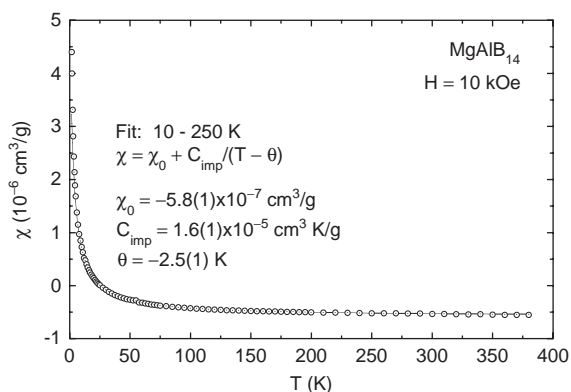


Fig. 7. Magnetic susceptibility χ versus temperature T of a MgAlB_{14} powder sample which contained approximately 20 ± 5 wt% MgAl_2O_4 (\odot). The solid curve is a fit to the data by the function shown in the figure [Eq. (3)], with parameters also listed in the figure.

is the sum of the contribution from the diamagnetic cores of the atoms, χ^{core} , and the paramagnetic Van Vleck susceptibility, χ^{VV} , which is expected to be small in this non-transition metal compound. The fit yielded $\theta = -2.5(1) \text{ K}$, $C_{\text{imp}} = 1.6(1) \times 10^{-5} \text{ cm}^3 \text{ K/g}$, and $\chi_0 = -5.8(1) \times 10^{-7} \text{ cm}^3/\text{g}$.

To analyze the contribution of χ^{core} to χ_0 , we assumed that the sample was made up of 20 wt% MgAl_2O_4 and 80 wt% MgAlB_{14} . Diamagnetic core susceptibilities χ^{core} tabulated in Ref. [28] were used for Mg^{+2} ($-3 \times 10^{-6} \text{ cm}^3/\text{mol}$), Al^{+3} ($-2 \times 10^{-6} \text{ cm}^3/\text{mol}$), and O^{-2} ($-12 \times 10^{-6} \text{ cm}^3/\text{mol}$). Further analysis depends strongly on the assumed χ^{core} of B. Using the Pascal constant for B tabulated in Ref. [29], $-7.2 \times 10^{-6} \text{ cm}^3/\text{mol B}$, yielded a calculated χ_0 value for MgAlB_{14} most consistent with the value obtained from the fit. The value of χ^{core} for 1 mol of MgAl_2O_4 is

$$\begin{aligned} \chi^{\text{core}}(\text{MgAl}_2\text{O}_4) &= -5.5 \times 10^{-5} \text{ cm}^3/\text{mol} \\ &= -3.9 \times 10^{-7} \text{ cm}^3/\text{g}. \end{aligned} \quad (5)$$

The value of χ^{core} for 1 mol of MgAlB_{14} is

$$\begin{aligned} \chi^{\text{core}}(\text{MgAlB}_{14}) &= -1.06 \times 10^{-4} \text{ cm}^3/\text{mol} \\ &= -5.2 \times 10^{-7} \text{ cm}^3/\text{g}. \end{aligned} \quad (6)$$

The calculated value of χ^{core} for our sample is

$$\begin{aligned} \chi_{\text{calc.}}^{\text{core}} &= 0.2(-3.9 \times 10^{-7} \text{ cm}^3/\text{g}) \\ &\quad + 0.8(-5.2 \times 10^{-7} \text{ cm}^3/\text{g}) \\ &= -7.8 \times 10^{-8} \text{ cm}^3/\text{g} + -4.2 \times 10^{-7} \text{ cm}^3/\text{g} \\ &= -4.9 \times 10^{-7} \text{ cm}^3/\text{g}, \end{aligned} \quad (7)$$

which is slightly more positive than the value obtained from the fit, $-5.8(1) \times 10^{-7} \text{ cm}^3/\text{g}$. The value of χ^{VV} from Eq. (4) is thus small as expected: $\chi^{\text{VV}} \cong 8.6 \times 10^{-8} \text{ cm}^3/\text{g}$ of sample.

4. Magnetization of hot pressed MgAlB₁₄

The magnetization $M(T)$ in an applied magnetic field of $H = 10 \text{ kOe}$ for a typical hot pressed MgAlB₁₄ sample is shown in Fig. 8. The data are qualitatively different from the data for powder MgAlB₁₄ shown in Fig. 7 and are indicative of ferromagnetism with a saturation moment $M_s \simeq 0.4 \mu_B/\text{FU}$. The Curie temperature T_c was estimated to be $\sim 460 \text{ K}$ by drawing a line through the region of maximum slope as shown in the figure. A magnetization M versus magnetic field H isotherm at $T = 300 \text{ K}$ is shown in Fig. 9. The magnetization nearly saturates at fields above 1 T. The saturation moment M_s was obtained by fitting the 4–5.5 T data with Eq. (1), yielding $M_s =$

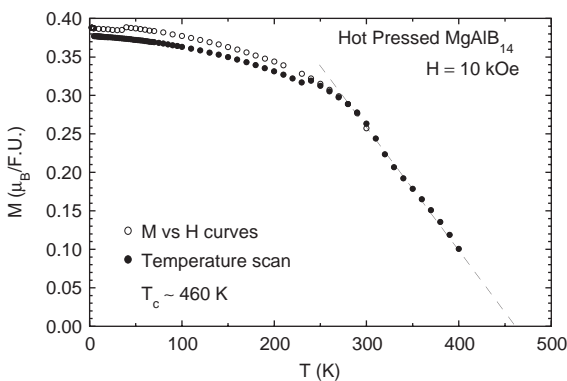


Fig. 8. Magnetization M versus temperature T of hot pressed MgAlB₁₄. The solid circles (●) were taken by scanning the temperature in a fixed magnetic field of $H = 10 \text{ kOe}$. The open circles (○) are 10 kOe data from $M(H)$ curves taken at fixed temperature. A dashed line drawn through the region of maximum slope was used to estimate $T_c \sim 460 \text{ K}$, as shown.

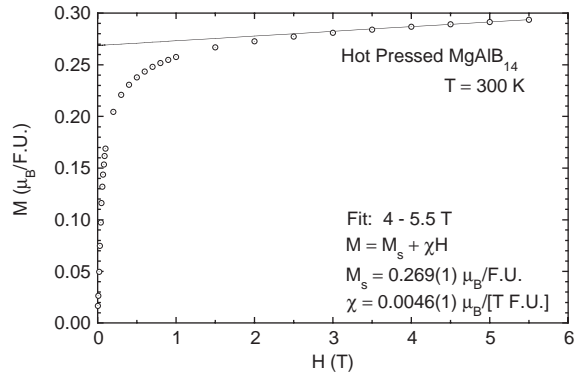


Fig. 9. Magnetization M versus magnetic field H at 300 K of hot pressed MgAlB₁₄ (○). The solid curve is a fit to the high field data by the function shown in the figure [Eq. (1)], with parameters also listed in the figure.

$0.269(1) \mu_B/\text{FU}$, equivalent to the contribution of $\sim 12 \text{ mol}\%$ Fe metal impurities, and $\chi = 0.0046(1) \mu_B/[\text{T FU}]$. For comparison, the drastically different $M(H)$ isotherm at $T = 300 \text{ K}$ for a powder sample of MgAlB₁₄ was shown in Fig. 6.

Since the magnetization shows a significant saturation moment, isothermal $M(H)$ hysteresis loop data were obtained. A hysteresis loop taken at $T = 300 \text{ K}$ for the hot pressed material is shown in Fig. 10. The remnant magnetization and coercive field are small, $0.0485 \mu_B/\text{FU}$ and $\sim 75 \text{ Oe}$, respectively.

The $M(T)$ in an applied magnetic field of $H = 10 \text{ kOe}$ for a hot pressed sample of nominal composition $\text{MgAl}_{0.95}\text{Si}_{0.05}\text{B}_{14}$ is shown in Fig. 11. The data are very similar to those for the unsubstituted hot pressed sample and indicate a ferromagnetic transition. The Curie temperature as estimated from the dashed line shown in the figure is $T_c \sim 335 \text{ K}$. An $M(H)$ isotherm at $T = 300 \text{ K}$ is shown in Fig. 12. A fit to the 4–5.5 T data by Eq. (1) yielded $M_s = 0.086(1) \mu_B/\text{FU}$, equivalent to the contribution of $\sim 4 \text{ mol}\%$ Fe metal impurities, and $\chi = 0.00297(8) \mu_B/[\text{T FU}]$.

An $M(H)$ isotherm at $T = 300 \text{ K}$ for a hot pressed sample with nominal composition $(\text{MgAlB}_{14})(\text{TiB}_2)_{1,3}$ is shown in Fig. 13. The data for this TiB₂ doped sample are very similar to the other samples, suggesting a significant contribution to the magnetization arises from

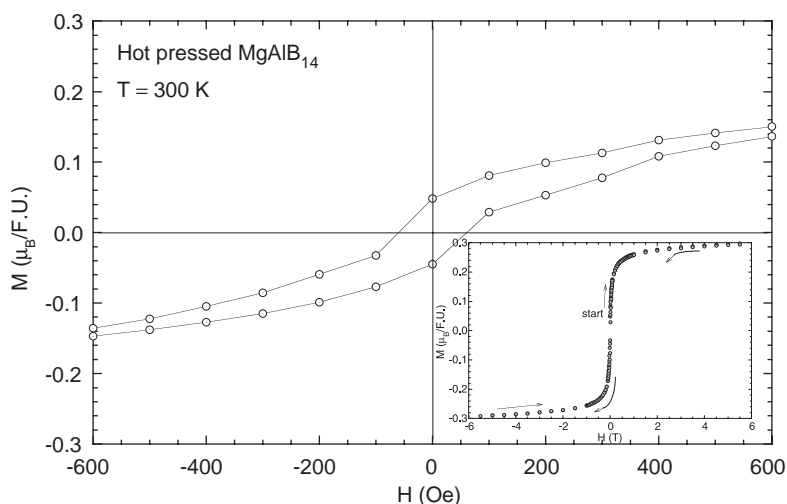


Fig. 10. An $M(H)$ hysteresis loop at 300 K of hot pressed MgAlB_{14} (\odot) in the low-field regime. The inset shows the entire loop with a maximum applied magnetic field of 5.5 T.

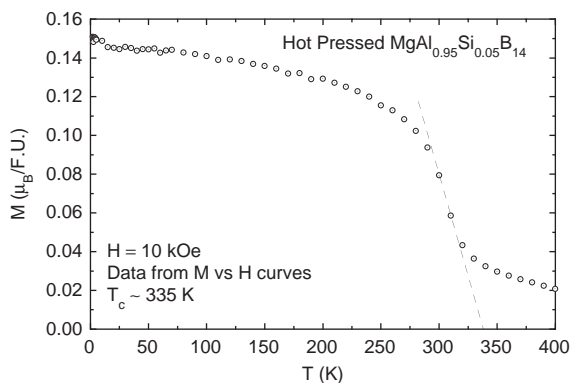


Fig. 11. Magnetization M versus temperature T of a hot pressed sample of nominal composition $\text{MgAl}_{0.95}\text{Si}_{0.05}\text{B}_{14}$ (\odot). The 10 kOe data were taken from isothermal $M(H)$ curves. A dashed line drawn through the region of maximum slope was used to estimate $T_c \sim 335$ K, as shown.

ferromagnetic impurities. A fit to the 4–5.5 T data by Eq. (1) yielded $M_s = 0.2709(4)\mu_B/\text{FU}$, equivalent to the contribution of ~ 12 mol% Fe metal impurities, and $\chi = 0.00177(3)\mu_B/[\text{T FU}]$.

5. Summary and conclusions

Single phase powder samples of MgAlB_{14} were not obtained by the conventional solid state synthesis method employed here. Significant

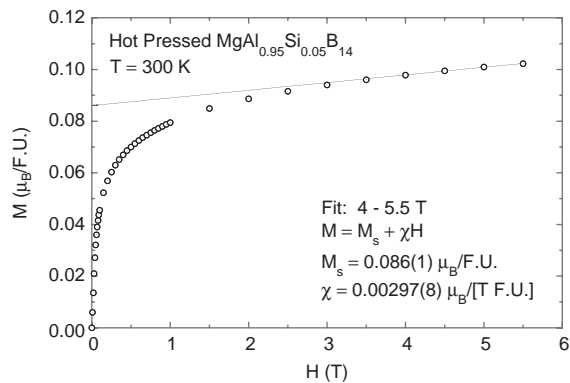


Fig. 12. Magnetization M versus magnetic field H at 300 K of a hot pressed sample of nominal composition $\text{MgAl}_{0.95}\text{Si}_{0.05}\text{B}_{14}$ (\odot). The solid curve is a fit to the high field data by the function shown in the figure [Eq. (1)], with parameters also listed in the figure.

amounts of both MgAl_2O_4 and AlB_{12} were formed in various samples as secondary phases according to XRD analysis. The magnetic susceptibility χ of our highest purity powder sample showed temperature-independent diamagnetism plus a paramagnetic Curie–Weiss contribution equivalent to that of approximately 1 mol% of spin- $\frac{1}{2}$ impurities.

The nominally pure hot pressed MgAlB_{14} samples and samples containing additional Si or TiB_2 were found to contain varying amounts of Fe impurities. Based on transmission electron

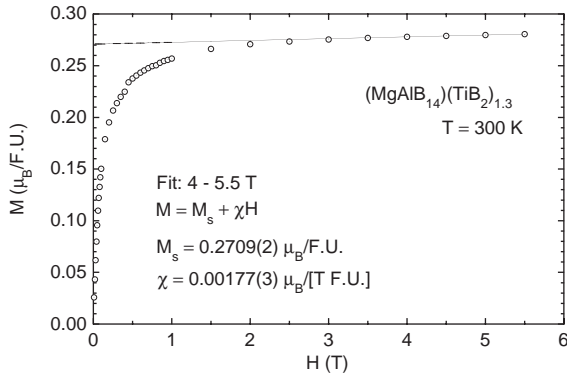


Fig. 13. Magnetization M versus magnetic field H at 300 K of a hot pressed sample of nominal composition $(\text{MgAlB}_{14})(\text{TiB}_2)_{1.3}$ (\odot). The solid curve is a fit to the high field data by the function shown in the figure [Eq. (1)], with parameters also listed in the figure.

microscopy images of samples substituted with TiB_2 , selected area diffraction with resolution of order 200 nm was performed, yielding distinct TiB_2 areas separate from MgAlB_{14} areas [30]. We, therefore, conclude that TiB_2 did not act as a traditional dopant, but rather primarily collected in boride phases in the grain boundaries. Based on the results of the SEM and Auger microprobe analyses, we conclude that the Fe impurity content is sufficient to account for the observed ferromagnetism in the magnetization data.

Lee and Harmon (Ref. [31]) have calculated the elastic constants of MgAlB_{14} . The measured hardness for the hot pressed samples (Ref. [11]) is larger than they calculated. Therefore, the Fe and other dopants acting in conjunction with an ultrafine microstructure may increase the hardness of this compound. It is therefore of interest to synthesize single phase MgAlB_{14} so that the intrinsic hardness and elastic constants can be measured. Magnetization measurements on a single-phase sample would also facilitate a better determination of the intrinsic magnetic behavior.

Acknowledgements

Ames Laboratory is operated for the US Department of Energy by Iowa State University

under Contract No. W-7405-Eng-82. This work was supported by the Director for Energy Research, Office of Basic Energy Sciences.

References

- [1] J. Nagamatsu, N. Nakagawa, T. Muranaka, Y. Zenitani, J. Akimitsu, *Nature* 410 (2001) 63.
- [2] C. Buzea, T. Yamashita, *Supercond. Sci. Technol.* 14 (2001) R115 and cited references.
- [3] J. Bardeen, L.N. Cooper, J.R. Schrieffer, *Phys. Rev.* 108 (5) (1957) 1175.
- [4] T. Masui, K. Yoshida, S. Lee, A. Yamamoto, S. Tajima, *Phys. Rev. B* 65 (2002) 214513.
- [5] H. Kotegawa, K. Ishida, Y. Kitaoka, T. Muranaka, N. Nakagawa, H. Takigawa, J. Akimitsu, *Phys. Rev. B* 66 (2002) 064516.
- [6] N.W. Ashcroft, N.D. Mermin, *Solid State Physics*, W.B. Saunders Company, Philadelphia, PA, 1976.
- [7] C. Kittel, *Introduction to Solid State Physics*, 7th Edition, Wiley, New York, 1996.
- [8] D.P. Young, D. Hall, M.E. Torelli, Z. Fisk, J.L. Sarrao, J.D. Thompson, H.-R. Ott, S.B. Oseroff, R.G. Goodrich, R. Zysler, *Nature* 397 (1999) 412.
- [9] S. Otani, T. Mori, *J. Phys. Soc. Jpn.* 71 (7) (2002) 1791.
- [10] K. Taniguchi, T. Katsufuji, F. Sakai, H. Ueda, K. Kitazawa, H. Takagi, *Phys. Rev. B* 66 (2002) 064407.
- [11] B.A. Cook, J.L. Harringa, T.L. Lewis, A.M. Russell, *Scr. Mater.* 42 (2000) 597.
- [12] J.C. Anderson, K.D. Leaver, R.D. Rawlings, J.M. Alexander, *Materials Science*, 4th Edition, Chapman & Hall, London, 1990, p. 212.
- [13] J. de Launay, The theory of specific heats and lattice vibrations, in: F. Seitz, D. Turnbull (Eds.), *Solid State Physics*, Vol. 2, Academic Press Inc., New York, 1956, p. 233.
- [14] V.I. Matkovich, *J. Economy, Acta Crystallogr. Sect. B* 26 (1970) 616.
- [15] I. Higashi, T. Ito, *J. Less-Common Met.* 92 (1983) 239.
- [16] I. Higashi, M. Kobayashi, S. Okada, K. Hamano, T. Lundström, *J. Cryst. Growth* 128 (1993) 1113.
- [17] M.M. Korsukova, V.N. Gurin, Y.B. Kuzma, N.F. Chaban, S.I. Chykhrii, V.V. Moshchalkov, N.B. Brandt, A.A. Gippius, K. Khyu Nyan, *Phys. Stat. Sol. A* 114 (1989) 265.
- [18] M.M. Korsukova, V.N. Gurin, Y. Yu, L.-E. Tergenius, T. Lundström, *J. Alloys Compounds* 190 (1993) 185.
- [19] M.M. Korsukova, T. Lundström, L.-E. Tergenius, V.N. Gurin, *J. Alloys Compounds* 187 (1992) 39.
- [20] A. Guette, M. Barret, R. Naslain, P. Hagenmuller, *J. Less-Common Met.* 82 (1981) 325.
- [21] I.A. Bairamashvili, L.I. Kekelidze, O.A. Golikova, V.M. Orlov, *J. Less-Common Met.* 67 (1979) 461.
- [22] O.A. Golikova, S. Samatov, *Phys. Stat. Sol. A* 77 (1983) 449.

- [23] M.M. Kazanin, V.V. Kutasov, *Phys. Stat. Sol. A* 113 (1989) 143.
- [24] M. Takeda, F. Domingo, T. Miura, T. Fukuda, *Mater. Res. Soc. Symp. Proc.* 691 (2002) 209.
- [25] H. Werheit, U. Kuhlmann, G. Krach, I. Higashi, T. Lundström, Y. Yu, *J. Alloys Compounds* 202 (1993) 269.
- [26] N.V. Vekshina, L.Y. Markovskii, Y.D. Kondrashev, T.K. Voevodskaya, *Zh. Prikl. Khim.* 44 (5) (1971) 958; *J. Appl. Chem. USSR* 44 (1971) 970.
- [27] A.M. Russell, B.A. Cook, J.L. Harringa, T.L. Lewis, *Scr. Mater.* 46 (2002) 629.
- [28] P.W. Selwood, *Magnetochemistry*, 2nd Edition, Interscience, New York, 1956, p. 78.
- [29] E. König, G. König, Magnetic properties of coordination and organometallic transition metal compounds, in: K.-H. Hellwege, A.M. Hellwege (Eds.), *Landolt-Börnstein: Numerical Data and Functional Relationships in Science and Technology*, Vol. 8, Springer, Berlin, 1976.
- [30] T.L. Lewis, A.M. Russell, B.A. Cook, J.L. Harringa, *Mater. Sci. Eng. A*, in press.
- [31] Y. Lee, B.N. Harmon, *J. Alloys Compounds* 338 (2002) 242.